## **OPEN ACCESS**



# Deep XMM-Newton Observations of an X-ray Weak Broad Absorption Line Quasar at z = 6.5

Jinyi Yang <sup>1,8</sup>, Xiaohui Fan <sup>1</sup>, Feige Wang <sup>1,9</sup>, Giorgio Lanzuisi <sup>2</sup>, Riccardo Nanni <sup>3</sup>, Massimo Cappi <sup>2</sup>, George Chartas <sup>4</sup>, Mauro Dadina <sup>2</sup>, Roberto Decarli <sup>2</sup>, Xiangyu Jin <sup>1</sup>, Charles R. Keeton <sup>5</sup>, Bram P. Venemans <sup>6</sup>, Fabian Walter <sup>6</sup>, Ran Wang <sup>7</sup>, Xue-Bing Wu <sup>7</sup>, Minghao Yue <sup>1</sup>, and Ann Zabludoff <sup>1</sup>, Steward Observatory, University of Arizona, 933 N. Cherry Avenue, Tucson, AZ 85721, USA; jinyiyang @email.arizona.edu <sup>2</sup> INAF—Osservatorio di Astrofisica e Scienza dello Spazio di Bologna, via Gobetti 93/3, I-40129 Bologna, Italy <sup>3</sup> Leiden Observatory, Leiden University, P.O. Box 9513, NL-2300 RA Leiden, The Netherlands <sup>4</sup> Department of Physics and Astronomy of the College of Charleston, Charleston, SC 29424, USA <sup>5</sup> Department of Physics and Astronomy, Rutgers University, Piscataway, NJ 08854, USA <sup>6</sup> Max-Planck Institute for Astronomy, Königstuhl 17, D-69117 Heidelberg, Germany <sup>7</sup> Kavli Institute for Astronomy and Astrophysics, Peking University, Beijing 100871, People's Republic of China Received 2021 October 22; revised 2021 December 16; accepted 2021 December 19; published 2022 January 12

#### Abstract

We report X-ray observations of the most distant known gravitationally lensed quasar, J0439+1634 at z=6.52, which is also a broad absorption line (BAL) quasar, using the XMM-Newton Observatory. With a 130 ks exposure, the quasar is significantly detected as a point source at the optical position with a total of  $358^{+19}_{-19}$  net counts using the EPIC instrument. By fitting a power law plus Galactic absorption model to the observed spectra, we obtain a spectral slope of  $\Gamma=1.45^{+0.10}_{-0.09}$ . The derived optical-to-X-ray spectral slope  $\alpha_{\rm ox}$  is  $-2.07^{+0.01}_{-0.01}$ , suggesting that the X-ray emission of J0439+1634 is weaker by a factor of 18 than the expectation based on its 2500 Å luminosity and the average  $\alpha_{\rm ox}$  versus luminosity relationship. This is the first time that an X-ray weak BAL quasar at z>6 has been observed spectroscopically. Its X-ray weakness is consistent with the properties of BAL quasars at lower redshift. By fitting a model including an intrinsic absorption component, we obtain intrinsic column densities of  $N_{\rm H}=2.8^{+0.7}_{-0.6}\times10^{23}\,{\rm cm}^{-2}$  and  $N_{\rm H}=4.3^{+1.8}_{-1.5}\times10^{23}\,{\rm cm}^{-2}$ , assuming a fixed  $\Gamma$  of 1.9 and a free  $\Gamma$ , respectively. The intrinsic rest-frame 2–10 keV luminosity is derived as  $(9.4-15.1)\times10^{43}\,{\rm erg\,s}^{-1}$ , after correcting for lensing magnification ( $\mu=51.3$ ). The absorbed power-law model fitting indicates that J0439+1634 is the highest redshift obscured quasar with a direct measurement of the absorbing column density. The intrinsic high column density absorption can reduce the X-ray luminosity by a factor of 3–7, which also indicates that this quasar could be a candidate intrinsically X-ray weak quasar.

Unified Astronomy Thesaurus concepts: Quasars (1319); X-ray quasars (1821); Early universe (435)

## 1. Introduction

Reionization-era quasars are direct probes of supermassive black hole (SMBH) and massive galaxy assembly in the early universe. Recent successful high-redshift quasar surveys provide a large sample of new reionization-era quasars (e.g., Venemans et al. 2015; Bañados et al. 2018; Matsuoka et al. 2019; Reed et al. 2019; Wang et al. 2019; Yang et al. 2019b). Near-infrared (NIR) spectroscopy of these quasars has revealed the existence of billion solar mass BHs within the first Gyr after the Big Bang and has also suggested that these SMBHs are accreting close to the Eddington limit (e.g., Shen et al. 2019; Schindler et al. 2020; Yang et al. 2021). X-ray emission from high-redshift quasars probes the conditions in the innermost regions of their accretion-disk corona, and thus provides information about how these early SMBHs are fed.

There have been substantial efforts to conduct multiwavelength observations of the most distant quasars; their properties in the optical, NIR, to (sub)millimeter bands have

Original content from this work may be used under the terms of the Creative Commons Attribution 4.0 licence. Any further distribution of this work must maintain attribution to the author(s) and the title of the work, journal citation and DOI.

been well characterized. However, studies of the X-ray properties of these systems are still limited. There are  $\sim 30$ quasars detected in X-rays at z > 6 (e.g., Shemmer et al. 2006; Moretti et al. 2014; Page et al. 2014; Ai et al. 2017; Gallerani et al. 2017; Nanni et al. 2017, 2018; Bañados et al. 2018; Connor et al. 2019, 2020; Vito et al. 2019; Wang et al. 2021) among more than 200 quasars known at this redshift, and only seven at z > 6.5 with X-ray detections (e.g., Page et al. 2014; Bañados et al. 2018; Vito et al. 2019; Connor et al. 2020; Pons et al. 2020; Wang et al. 2021). Due to their extreme distances, the observed X-ray emission of these quasars is very faint, and only four z > 6 quasars are detected with more than 100 net counts (Page et al. 2014; Ai et al. 2017; Nanni et al. 2017; Vito et al. 2019), which limits detailed investigations of their X-ray spectral properties and any correlations with other quasar properties. Recent studies of high-redshift quasars have mostly focused on their average X-ray properties. In addition, all previous X-ray observations have been obtained only for the most intrinsically luminous quasars, probing only the most massive SMBHs.

Quasar J0439+1634 at z=6.5188 is the first known gravitationally lensed quasar at z>5 and the brightest quasar known at this redshift at rest-frame UV/optical-to far-infrared wavelengths due to lensing. The high lensing magnification ( $\mu=51.3$ , Fan et al. 2019) makes J0439+1634 an ideal target for the study of X-ray emission from a reionization-era quasar

<sup>8</sup> Strittmatter Fellow.

<sup>&</sup>lt;sup>9</sup> NASA Hubble Fellow.

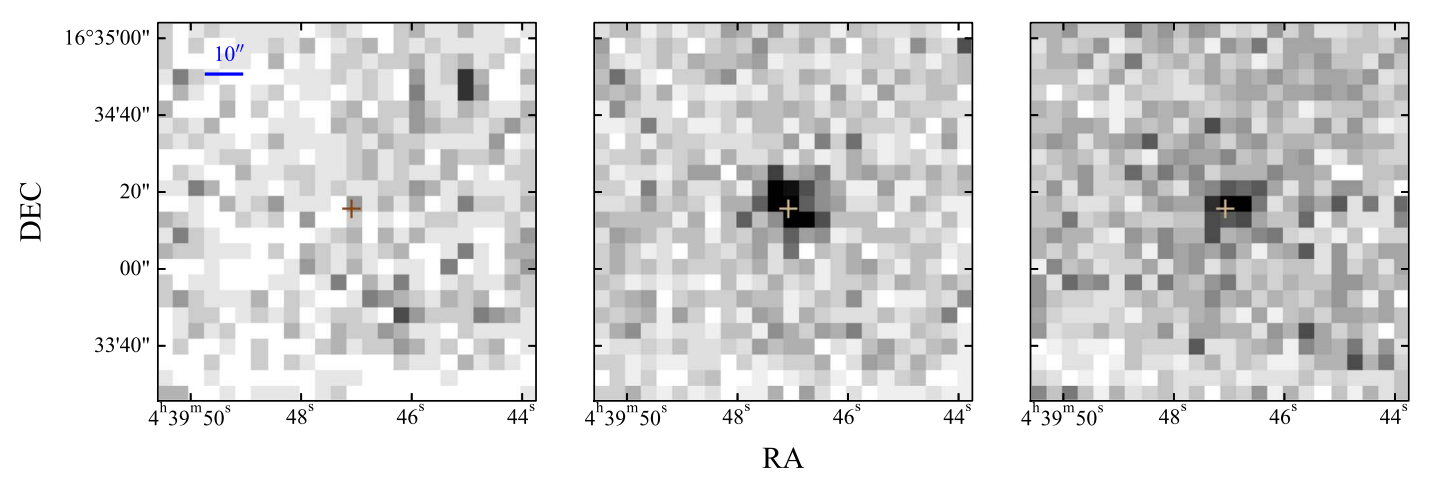


Figure 1. The XMM-Newton EPIC image  $(100'' \times 100'')$  of J0439+1634, combined from the pn, MOS1, and MOS2 images, in the 0.2–0.5 keV (left), 0.5–2 keV (middle), and 2–10 keV (right) X-ray bands. The central crosses represent the optical coordinates of this quasar (i.e., J043947.08+163415.7, Fan et al. 2019). The quasar is detected in the 0.5–2 keV (rest-frame 3.8–15 keV) and 2–10 keV (rest-frame 15–75 keV) bands, but not in the 0.2–0.5 keV band (rest-frame 1.5–3.8 keV).

that is intrinsically less luminous. In addition, this quasar is also a broad absorption line (BAL) quasar (Yang et al. 2021). BAL quasars have been suggested to be highly absorbed in the soft X-ray band and are generally X-ray weak in observations of low-redshift quasars; no such studies of high-redshift BAL quasars have been carried out, due to their faint X-ray emission. In this work, we report XMM-Newton observations of J0439 +1634. We investigate its X-ray properties through spectral analysis and compare it with other high-redshift and low-redshift quasar populations. All results below refer to a  $\Lambda$ CDM cosmology with parameters  $\Omega_{\Lambda} = 0.7$ ,  $\Omega_{m} = 0.3$ , and h = 0.7.

#### 2. XMM-Newton Observations and Data Reduction

J0439+1634 was observed with XMM-Newton on 2020 August 24 for a total observing time of 130 ks (Program ID 86320). The European Photon Imaging Camera (EPIC) was operated in full-frame mode, with thin filters. The EPIC data have been processed with XMM-Newton Science Analysis Software (SAS) v19.1.0 following the standard data analysis threads. 10 We filtered out time periods with high particle backgrounds by limiting the count-rate thresholds to <0.4 cts s<sup>-1</sup> in the 10 < E < 12 keV band light curves for the pn camera and <0.35 cts s<sup>-1</sup> in the E > 10 keV band for the MOS cameras. We only considered events with patterns 0-4 and 0-12 for the scientific analysis for the pn and MOS cameras, respectively. We created images and extracted spectra, response matrices, and ancillary files using the evselect, backscale, rmfgen, and arfgen tools. For spectral extraction, we extracted the counts from the three cameras separately. We extracted counts from circular regions centered at the optical position of the quasar with a radius of 12", and we selected an object-free nearby circular regions with a 60" radius for the background, 25 times larger than the target extraction area. We also group the spectra using specgroup with a minimum number of counts of one per bin, which will be used for spectral fitting. The total effective exposure times are 76.9 ks, 118.7 ks, and 118.6 ks for pn, MOS1, and MOS2, respectively. We merged the images from the three EPIC cameras using the merge tool, in three different observed bands, from soft to hard: 0.2–0.5 keV (rest-frame 1.5–3.8 keV), 0.5–2 keV (rest-frame

3.8–15 keV), and 2–10 keV (rest-frame 15–75 keV), as shown in Figure 1.

### 3. Results

## 3.1. X-Ray Detection and Spectra

An X-ray source is clearly detected at a position consistent with the optical coordinates of J0439+1634 (i.e., J043947.08 +163415.7, Fan et al. 2019) in 0.5-10 keV in all three EPIC cameras, while it is not detected in the 0.2-0.5 keV band (Figure 1) using edetect chain. The X-ray source is located 0".7-0".9 away from the optical coordinates in the pn and MOS1 images and 1"5 away in MOS2 (with a  $1\sigma$  uncertainty of  $\sim 0.98$  in all three images), based on *edetect\_chain*. The X-ray and optical coordinates overlap within the spatial resolution in the all three cameras. The target is detected with false source probabilities of less than  $3 \times 10^{-8}$  by all three cameras, derived using the binomial no-source probability (Broos et al. 2007; Weisskopf et al. 2007; Vito et al. 2019). In this lensing system, the foreground lensing galaxy is 0."5 to the East from the quasar, and the separation between the two lensed quasar images is about 0"2 in the HST image (Fan et al. 2019). Thus, the entire system is unresolved in the EPIC observations. HST and ground-based observations show that the foreground lens galaxy is a faint, low-mass galaxy (dynamical mass  $\sim 2\times 10^{10}\,M_\odot$  from the best-fit lensing model) without any hints of AGN activity (Fan et al. 2019; Yue et al. 2021). We therefore consider that all X-ray emission detected here is from the quasar. The number of total net counts from the three cameras is  $358^{+19}_{-19}$  in the 0.2–10 keV band. There are no other source detected within 50" of the quasar.

Figure 2 shows the spectra from the three EPIC cameras. There is a drop in the counts from  $\sim$ 0.8 keV to the soft end, which does not appear in other EPIC spectra of z>6 quasars (Moretti et al. 2014; Page et al. 2014; Ai et al. 2017; Nanni et al. 2017) and potentially indicates strong absorption in the rest-frame soft band. We apply spectral fitting to the data that have been grouped into one count per bin using XSPEC with the Cash statistic (Cash 1979). When fitting, we fix the Galactic HI column density to  $N_{\rm H}$  of  $1.46 \times 10^{21}$  cm<sup>-2</sup>, derived based on the Leiden/Argentine/Bonn map (Kalberla et al. 2005).

We first fit the data with a power law plus Galactic absorption model (phabs\*zpowerlw in XSPEC) and obtain a best-fit

 $<sup>^{10}\</sup> https://www.cosmos.esa.int/web/xmm-newton/sas-threads$ 

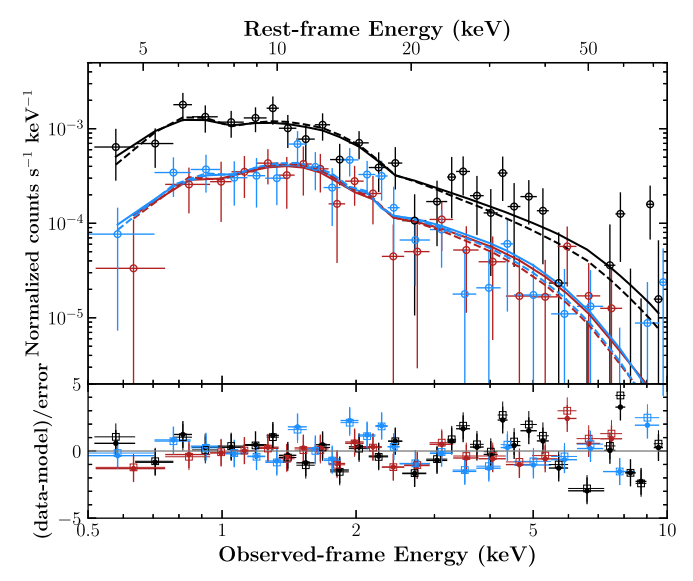
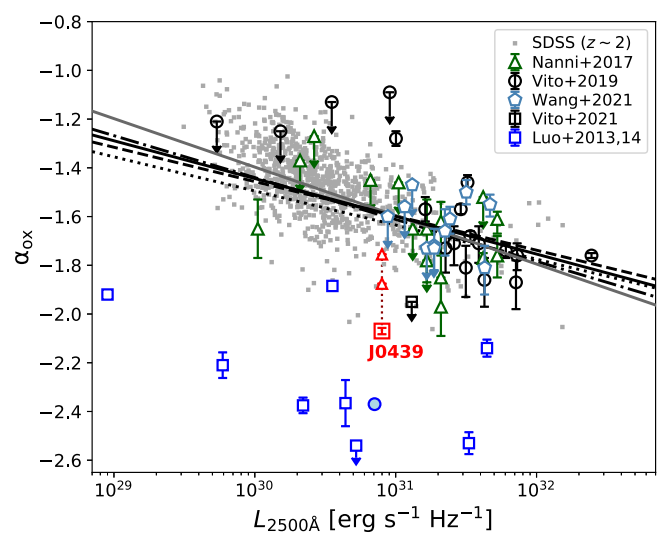


Figure 2. The XMM-Newton EPIC spectra of quasar J0439+1634. The upper panel shows the observed counts from the pn camera (black), MOS1 (red), and MOS2 (blue). The solid lines represent the spectral fits using an absorbed power-law model consistent of a power-law model, Galactic absorption, and quasar intrinsic absorption, with the assumption of an intrinsic photon index of  $\Gamma=1.9$  (Nanni et al. 2017). The dashed lines denote the spectral fits with a free  $\Gamma$  (see details of spectral fitting in Section 3.2). The bottom panel shows the residuals, with filled circles for the fixed- $\Gamma$  fits and open squares for the  $\Gamma$ -free fits. The spectral fitting is applied to the spectra grouped to one count per bin, and the data have been rebinned for plotting purpose here using XSPEC.

photon index of  $\Gamma=1.45^{+0.10}_{-0.09}$ , with a C statistic of 247.51 for 240° of freedom. The slope is flatter than the typical slopes for  $z\gtrsim 6$  quasars that have X-ray spectra (e.g.,  $\Gamma\sim 1.6$ –2.2, Page et al. 2014; Ai et al. 2017; Nanni et al. 2017; Vito et al. 2019); it is also flatter than the measurements for low-redshift quasars (e.g., Vignali et al. 2005; Just et al. 2007). Comparisons between radio-loud and radio-quiet quasars at lower redshift suggest a flatter slope ( $\Gamma\sim 1.55$ , e.g., Page et al. 2005) for radio-loud quasars than for radio-quiet quasars ( $\Gamma\sim 1.98$ , e.g., Page et al. 2005, also Scott et al. 2011). J0439+1634, however, is radio-quiet (Yang et al. 2019a).

Based on the spectral fitting results with the power-law model, we compute the Galactic absorption-corrected fluxes. The flux in the 0.5–2 keV band is  $4.9^{+0.3}_{-0.3}\times10^{-15}$  erg s $^{-1}$  cm $^{-2}$ , and the flux in the 2–10 keV band is  $13.1^{+0.8}_{-0.8}\times10^{-15}$  erg s $^{-1}$  cm $^{-2}$ . The rest-frame 2–10 keV band luminosity based by our fit is  $2.2^{+0.1}_{-0.1}\times10^{45}$  erg s $^{-1}$  without correction for magnification. After correction for magnification ( $\mu=51.3$ , Fan et al. 2019), the intrinsic rest-frame 2–10 keV band luminosity is  $4.3^{+0.3}_{-0.3}\times10^{43}$  erg s $^{-1}$ . We estimate the optical–X-ray power-law slope,  $\alpha_{\rm ox}$ , based on

We estimate the optical–X-ray power-law slope,  $\alpha_{\rm ox}$ , based on the flux densities at 2500 Å and 2 keV in the rest frame. The restframe 2 keV (0.266 keV in the observed frame) flux density is calculated using the PIMMS based on the Galactic absorption-corrected flux. The rest-frame 2500 Å flux density is derived from the NIR spectral fitting in Yang et al. (2021). We find a slope  $\alpha_{\rm ox}$  of  $-2.07^{+0.01}_{-0.01}$ . We then compare the measurement of J0439+1634 with the existing relations between  $\alpha_{\rm ox}$  and 2500 Å luminosity density and measurements in the literature. J0439+1634, with  $L_{2500\,\mathring{A}}=8.0\times10^{30}\,{\rm erg\,s^{-1}\,Hz^{-1}}$  after correcting for the lensing magnification, has an intrinsic luminosity significantly lower than most  $z\gtrsim6$  quasars previously studied in X-rays.



**Figure 3.** Optical-to-X-ray spectral slope  $\alpha_{ox}$  vs. 2500 Å luminosity. Our measurement from J0439+1634 is shown in red, compared with values from quasar samples at similar redhsift and lower redshift. The two red triangles are the  $\alpha_{ox}$  values accounting for the intrinsic absorption based on  $\Gamma$ -fixed (lower value) and  $\Gamma$ -free (upper value) model fitting. For high-redshift comparisons, we show individual measurements at 5.5 < z < 6 from Nanni et al. (2017), 6 < z < 6.5 from Vito et al. (2019), and z > 6.5 from Wang et al. (2021). We also include the new upper limit (black square) from a z = 6.515 quasar in Vito et al. (2021). The low-redshift SDSS quasar sample (gray dots) is generated based on the  $L_{2-10 \text{ keV}}$  from Timlin et al. (2020) and  $L_{2500 \text{ Å}}$  from Wang et al. (2021). The relations in the literature are plotted as black solid line (Nanni et al. 2017), gray solid line (Timlin et al. 2020), dashed line (Lusso & Risaliti 2017), dotted line (Just et al. 2007), and dashed-dotted line (Martocchia et al. 2017). The blue squares are the measurements for lowredshift BAL quasars from Luo et al. (2014). Among the sample in Luo et al. (2014), the quasar PG0043+03 is not detected, and it has been updated in Kollatschny et al. (2016) (blue filled circle). All measurements have been corrected to the cosmology adopted in this work.

J0439+1634 is far below the  $\alpha_{ox}$ - $L_{2500\,\text{Å}}$  relations derived from low redshift and  $z \gtrsim 6$  quasar samples in the literature (e.g., Just et al. 2007; Lusso & Risaliti 2017; Martocchia et al. 2017; Nanni et al. 2017; Timlin et al. 2020; Bisogni et al. 2021), as shown in Figure 3, suggesting a much fainter X-ray luminosity from this quasar relative to its UV luminosity. Using the intrinsic continuum luminosity  $L_{2500\,\mathring{A}}$  of J0439 +1634 and applying the existing relation between  $\alpha_{ox}$  and 2500 A luminosity density from Nanni et al. (2017), we find that the expected rest-frame 2 keV luminosity should be 18 times higher than the observation. J0439+1634 is one of the highest redshift X-ray weak quasars and the only such object with high-quality X-ray spectroscopy at  $z \gtrsim 6.5$ , during the epoch of reionization. There are some other high-redshift quasars without X-ray detections, which could thus be candidates of X-ray weak quasars. In particular, Vito et al. (2021) report an upper limit on X-ray emission from a z = 6.515 quasar and suggest that its X-ray emission is >6 times weaker than the expectation based on UV luminosity.

## 3.2. High Obscuration

As discussed above, we obtain a flat spectral slope and faint X-ray luminosity for J0439+1634. To further investigate the nature of its weak X-ray emission, we perform additional spectral fits with models including more components. We apply spectral fitting using an absorbed power-law model (phabs\*zphabs\*zpowerlw in XSPEC) to estimate the

**Table 1**Best-fit Results of EPIC Spectra

| Model<br>(1)                           | C-stat/d.o.f. (2) | Γ<br>(3)               | N <sub>H</sub> (4)  | f <sub>(0.5-2 keV)</sub> (5) | f <sub>(2-10 keV)</sub> (6) | $\frac{L_{(2-10 \text{ keV,rest})}}{(7)}$ |
|--|-------------------|------------------------|---------------------|------------------------------|-----------------------------|---|
| Power law                              | 247.51/240        | $1.45^{+0.10}_{-0.09}$ | •••                 | $4.9^{+0.3}_{-0.3}$          | $13.1^{+0.8}_{-0.8}$        | $2.2^{+0.1}_{-0.1}$                       |
| Power law plus absorption <sup>a</sup> | 199.34/240        | 1.9                    | $2.8^{+0.7}_{-0.6}$ | $4.9^{+0.3}_{-0.3}$          | $11.1^{+0.7}_{-0.7}$        | $4.8^{+0.3}_{-0.3}$                       |
| Power law plus absorption <sup>b</sup> | 197.99/240        | 2.13                   | $3.9^{+0.7}_{-0.7}$ | $4.9^{+0.3}_{-0.3}$          | $9.9^{+0.6}_{-0.6}$         | $6.8^{+0.4}_{-0.4}$                       |
| Power law plus absorption <sup>c</sup> | 197.91/239        | $2.21^{+0.30}_{-0.26}$ | $4.3^{+1.8}_{-1.5}$ | $4.9^{+0.3}_{-0.3}$          | $9.5^{+0.6}_{-0.6}$         | $7.7^{+0.5}_{-0.5}$                       |

**Notes.** Columns: (1) model used for the spectral fitting, (2) C statistic/degrees of freedom, (3) best-fit or fixed photon index, (4) intrinsic absorption, in units of  $10^{23}$  cm<sup>-2</sup>, (5) and (6) fluxes in the observed 0.5–2 and 2–10 keV bands in units of  $10^{-15}$  erg cm<sup>-2</sup> s<sup>-1</sup>, corrected for Galactic absorption only, (7) rest-frame 2–10 keV band luminosity in units of  $10^{45}$  erg s<sup>-1</sup>, derived from the model and corrected for the Galactic absorption and intrinsic absorption (if applied), without correction for lensing magnification.

quasar intrinsic absorption, accounting for the same fixed Galactic absorption as above. We first assume an intrinsic photon index of  $\Gamma = 1.9$ , which is the average value derived from a  $z \sim 6$  quasar sample (Nanni et al. 2017) and also consistent with that of quasars at lower redshift (Vignali et al. 2005; Just et al. 2007). We find an intrinsic absorption of  $N_{\rm H}$  of  $2.8^{+0.7}_{-0.6} \times 10^{23}$  cm<sup>-2</sup> with a C statistic of 199.34 for 240° of freedom, resulting in an intrinsic rest-frame 2–10 keV band luminosity of  $9.4^{+0.6}_{-0.6} \times 10^{43}~\rm erg~s^{-1}$  (corrected for magnification). The Galactic absorption-corrected flux in the  $0.5-2~\rm keV$  band is  $4.9^{+0.3}_{-0.3}\times10^{-15}~\rm erg~s^{-1}~cm^{-2}$ , and the flux in the  $2-10~\rm keV$  band is  $11.1^{+0.7}_{-0.7}\times10^{-15}~\rm erg~s^{-1}~cm^{-2}$ . The best-fit is shown in Figure 2. As a test, we also fix  $\Gamma$  to 2.13, which is the average photon index from sources with >30 counts in the z > 6 quasar sample in Vito et al. (2019). This value is also similar to the average slope in Vito et al. (2019) for sources with <30 counts and to the average value for z > 6.5 quasars in Wang et al. (2021). Both of these two works suggest an increased photon index for quasars at z > 6. With this  $\Gamma$  value, we obtain a  $N_{\rm H}$  of  $3.9^{+0.7}_{-0.7} \times 10^{23}$  cm<sup>-2</sup> (C-stat/d.o.f. = 197.99/ 240), consistent with the best-fit results using  $\Gamma = 1.9$  within  $1\sigma$ uncertainty.

We then perform spectral fitting using the same absorbed power-law model but with a free  $\Gamma$ . In this case, we find a  $\Gamma$  of  $2.21^{+0.30}_{-0.26}$ , with relatively large uncertainty. The best-fit intrinsic absorption,  $N_{\rm H}=4.3^{+1.8}_{-1.5}\times10^{23}~{\rm cm}^{-2}$ , is also more loosely constrained than in the  $\Gamma$ -fixed cases. We then obtain an intrinsic rest-frame 2–10 keV band luminosity of  $15.1^{+1.0}_{-0.9}\times10^{43}~{\rm erg\,s}^{-1}$ . All fitting results show a high intrinsic column density,  $N_{\rm H}>2\times10^{23}~{\rm cm}^{-2}$ , which suggests that J0439+1634 is a highly obscured quasar but not yet Compton-thick. This is the highest redshift obscured quasar with direct measurement of the absorbing column density. These fitting results are summarized in Table 1. If we re-compute the rest-frame 2 keV luminosity taking into account both Galactic absorption and intrinsic absorption based on the best fits of absorbed power-law models, we find that the intrinsic 2 keV luminosity increases by  $\sim$ 3 times for the fixed  $\Gamma=1.9$  fit and  $\sim$ 7 times for the  $\Gamma$ -free fit.

Since J0439+1634 is a gravitationally lensed quasar, we also consider the foreground lensing galaxy as a possible source responsible for the absorption. We use the same absorbed power-law model and fix the redshift of zphabs component to 0.67, the best-fit redshift for the foreground lensing galaxy (Fan et al. 2019). In this case, we find a column density of  $N_{\rm H}=5.8^{+1.5}_{-1.3}\times10^{21}~{\rm cm}^{-2}$  with a fixed  $\Gamma=1.9$ , and

 $N_{\rm H}=6.2^{+2.5}_{-2.1}\times10^{21}~{\rm cm}^{-2}$  with  $\Gamma$ -free fitting. The lensing galaxy absorption can reduce the quasar intrinsic X-ray luminosity by a factor of  $\sim$ 3. Gaseous systems with such high column density will result in damped Ly $\alpha$  (DLA) absorptions in the quasar spectrum. Due to the low redshift of the lensing galaxy and the high redshift of the quasar, the absorption features, if they exist, would be at wavelengths far bluer than the quasar Lyman break, preventing direct detection of the DLA in the quasar spectrum. However, if a DLA system with this  $N_{\rm H}$  exists, we expect to see significant change in the quasar UV colors due to dust reddening:  $\sim 1$  mag extinction in the optical z band, assuming the mean dust-to-gas ratio of  $z \sim 0.7$ Mg II absorbers (Ménard & Chelouche 2009), which is a tracer of low-redshift DLAs. However, the rest-frame UV spectrum of J0439+1634, after correcting for the Galactic extinction, has a slope of  $\alpha_{\lambda} = -1.41$ , bluer than the mean (-1.2) of  $z \ge 6.5$ quasars (Yang et al. 2021). Therefore, it is not likely that there is a high column density absorbing system from the foreground lensing galaxy.

To consider the possible presence of an iron emission line at 6.4 keV, we also add to the absorbed power-law model a Gaussian line component. We fix the line rest-frame energy to 6.4 keV and line width to  $10 \, \text{eV}$  (e.g., Nanni et al. 2018). All the parameters of the other components are fixed to the best-fit values from the  $\Gamma$ -fixed ( $\Gamma$  = 1.9) or  $\Gamma$ -free fitting described above. We obtain an upper limit on line equivalent width of  $EW \leq 142 \, \text{eV}$  ( $\Gamma$ -fixed) and  $EW \leq 121 \, \text{eV}$  ( $\Gamma$ -free).

## 3.3. An X-ray Weak BAL Quasar

BAL quasars are known as a subclass of quasars seen with broad absorption features blueward of broad emission lines, which are thought to be evidence of high-velocity outflows from the accretion disk. X-ray observations of low-redshift BAL quasars show that they appear to be highly attenuated in the soft X-rays as the outflowing material could produce strong continuous absorption in X-rays. Previous studies of lowredshift BAL quasar samples report lower 2 keV luminosity (e.g., Brandt et al. 2000; Gibson et al. 2009; Luo et al. 2013, 2014; Liu et al. 2018) than the expectation from the  $\alpha_{\rm ox}$ – $L_{2500\,\mathring{A}}$  relation. Some works suggest that X-ray absorption is the primary cause of soft X-ray weakness in BAL quasars (e.g., Brandt et al. 2000; Gallagher et al. 2002), while there are also BAL quasars found as intrinsically X-ray weak quasars, for which the weakness is not entirely caused by absorption (e.g., Gibson et al. 2008; Luo et al. 2014; Liu et al. 2018).

<sup>&</sup>lt;sup>a</sup> Spectral fitting using absorbed power-law model with a fixed  $\Gamma$  of 1.9, the mean of  $z \gtrsim 6$  quasars in Nanni et al. (2017).

b Spectral fitting using absorbed power-law model with a fixed  $\Gamma$  of 2.13, the average photon index for z > 6 quasars in Vito et al. (2019).

 $<sup>^{\</sup>rm c}$  Spectral fitting using absorbed power-law model with free  $\Gamma$ .

The presence of BAL features in the UV/optical spectra of J0439+1634 (Yang et al. 2021) and its X-ray weakness relative to the  $\alpha_{\rm ox}$ - $L_{2500\,\mathring{A}}$  relation raise questions as to whether its X-ray weakness is related to its BAL properties: is it entirely due to absorption or is the quasar also intrinsically X-ray weak? As shown in Figure 3, J0439+1634 has X-ray properties different from the majority of high-redshift and lower-redshift quasars, but it has comparable X-ray weakness at 2 keV to that of BAL quasars. The drop at <0.8 keV (~6 keV in the rest frame) shown in Figure 2 and the flat  $\Gamma$  from our power-law fitting indicate absorption in the rest-frame soft band. The spectral fitting including absorption components shows a high column density, which suggests an absorption-caused weakness in the soft X-ray. As shown in Figure 3, correcting the X-ray spectra for intrinsic absorption based on the best fits of the absorbed power-law model will only increase the 2 keV luminosity by a factor of 3 and thus yield an  $\alpha_{ox}$  of -1.88 if assuming  $\Gamma = 1.9$ . If using the  $\Gamma$ -free fit, although with larger uncertainties, the correction can result in an  $\alpha_{ox}$  of -1.76, close to the expected value ( $\alpha_{\rm ox}=-1.58$ ) from the existing  $\alpha_{\rm ox}$ – $L_{2500\,\mathring{A}}$  relation. Therefore, if J0439 intrinsically has a steep  $\Gamma$ , the absorption is a sufficient explanation for its X-ray weakness. Otherwise, there is a possibility that the intrinsic absorption is not entirely responsible for the X-ray weakness, and J0439+1634 is a candidate of intrinsically X-ray weak BAL quasar.

Intrinsically X-ray weak quasars have been suggested to be rare. Gibson et al. (2008) find that the fraction of sources that are under luminous by a factor of 10 is  $\lesssim$ 2% among optically selected SDSS DR5 quasars. However, Liu et al. (2018) suggest a higher fraction (6%-23%) of intrinsically X-ray weak quasars among BAL population. There are studies suggesting that BAL windsrelated mechanisms could weaken or quench coronal X-ray emission (e.g., Proga 2005; Luo et al. 2013). A very high accretion rate is also discussed as one possible reason for the intrinsic X-ray weakness of BAL quasars (e.g., Leighly et al. 2007; Luo et al. 2014). Laurenti et al. (2021) recently report a high X-ray weak fraction ( $\sim$ 30%) among high-Eddington ratio AGN. For J0439+1634, its NIR spectral fitting shows an Eddington ratio  $(L_{\text{bol}}/L_{\text{Edd}})$  of  $0.6 \pm 0.1$   $(L_{\text{bol}} = (4.6 \pm 0.1) \times 10^{46} \text{ erg s}^{-1}$ ,  $M_{\rm BH} = (6.3 \pm 0.2) \times 10^8 \, M_{\odot}$ ), which is not high compared to the median value (i.e., 0.85; a mean of 1.08) for  $z \sim 6.5$  quasars (Yang et al. 2021). Another possible interpretation is that weak X-ray emission would not significantly ionize winds and thus intrinsically X-ray weak quasars have larger covering factors and are preferentially observed with BAL features (Liu et al. 2018). On the other hand, recent work by Nardini et al. (2019) find a large fraction ( $\sim$ 25%) of X-ray weak quasars in a sample of luminous blue radio-quiet, non-BAL quasars at  $z \sim 3$ , with no clear evidence of absorption.

Previous observations also show that low-ionization BAL quasars (LoBALs), which have BAL feature on low-ionization lines, such as Al III and Mg II, have lower 2 keV luminosity and higher absorbing column densities than high-ionization BAL quasars (HiBALs) (e.g., Green et al. 2001; Gallagher et al. 2002). Sameer et al. (2019) report different values of mean  $\Delta\alpha_{\rm ox}$  for HiBALs ( $\Delta\alpha_{\rm ox,mean}=-0.303$ ) and LoBALs ( $\Delta\alpha_{\rm ox,mean}=-0.587$ ). For J0439+1634, there is a weak Mg II absorption feature in its NIR spectrum, which is at the velocity corresponding to the strong C IV BAL absorption trough. Therefore it has low-ionization associated absorption, but with small velocity widths (<2000 km s^{-1}) of the Mg II absorption

compared to typical LoBALs. J0439+1634 has a  $\Delta\alpha_{\rm ox}$  of -0.45, between the average HiBAL and LoBAL values.

#### 4. Summary

We present XMM-Newton observations of a gravitationally lensed BAL quasar J0439+1634 at z = 6.5. With 130 ks of total observation time, the quasar is significantly detected with 358 net counts. Power-law-only spectral fitting of the EPIC spectra yields a flat photon index ( $\Gamma = 1.45^{+0.10}_{-0.09}$ ). This quasar is X-ray weak at rest-frame 2 keV relative to the expectation from the average  $\alpha_{\rm ox}$ - $L_{2500\,\mathring{A}}$  relation. It is underluminous by a factor of 18 in X-ray, consistent with the behavior of BAL quasars observed at lower redshift. Spectral fitting using an absorbed power-law model suggests a high intrinsic column density, with best-fit values of  $N_{\rm H}>2\times10^{23}~{\rm cm}^{-2}$  based on different  $\Gamma$ . J0439+1634 is therefore the first highly obscured quasar with X-ray spectroscopy in the reionization epoch, benefiting from its high lensing magnification. Accounting for a range of intrinsic absorption by assuming different  $\Gamma$ , we find that the 2 keV X-ray luminosity can increase by a factor of 3–7. The possible remaining X-ray weakness indicates that J0439+1634 could be a candidate of intrinsically X-ray weak quasar.

This research is based on observations obtained with XMM-Newton, an ESA science mission with instruments and contributions directly funded by ESA member states and NASA. J.Y., X.F., and M.Y. acknowledge support from US NSF grants AST 19-08284 and funding by NASA through a XMM Guest Observer program. F.W. acknowledges support from NASA through the NASA Hubble Fellowship grant #HF2-51448 awarded by the Space Telescope Science Institute, which is operated by the Association of Universities for Research in Astronomy, Incorporated, under NASA contract NAS5-26555. G.L., M.C., and M.D. acknowledge financial support from the Italian Space Agency under grant ASI-INAF I/037/12/0, and n. 2017-14-H.O. X.-B. W. acknowledges support from the National Key R&D Program of China (2016YFA0400703) and the National Science Foundation of China (11721303, 11890693). We thank Bin Luo for providing data from published works.

Facility: XMM-Newton.

*Software:* XMM-Newton Science Analysis Software (SAS) v19.1.0 (Gabriel et al. 2004), XSPEC (Arnaud 1996).

## **ORCID** iDs

Jinyi Yang https://orcid.org/0000-0001-5287-4242 Xiaohui Fan https://orcid.org/0000-0003-3310-0131 Feige Wang https://orcid.org/0000-0002-7633-431X Giorgio Lanzuisi https://orcid.org/0000-0001-9094-0984 Riccardo Nanni https://orcid.org/0000-0002-2579-4789 Massimo Cappi https://orcid.org/0000-0001-6966-8920 George Chartas https://orcid.org/0000-0003-1697-6596 Mauro Dadina https://orcid.org/0000-0002-7858-7564 Roberto Decarli https://orcid.org/0000-0002-2662-8803 Xiangyu Jin https://orcid.org/0000-0002-5768-738X Charles R. Keeton https://orcid.org/0000-0001-6812-2467 Bram P. Venemans https://orcid.org/0000-0001-9024-8322 Fabian Walter https://orcid.org/0000-0003-4793-7880 Ran Wang https://orcid.org/0000-0003-4956-5742 Xue-Bing Wu https://orcid.org/0000-0002-7350-6913 Minghao Yue https://orcid.org/0000-0002-5367-8021 Ann Zabludoff https://orcid.org/0000-0001-6047-8469

### References

```
Ai, Y., Fabian, A. C., Fan, X., et al. 2017, MNRAS, 470, 1587
Arnaud, K. A. 1996, in ASP Conf. Ser. 101, Astronomical Data Analysis
   Software and Systems V, ed. G. H. Jacoby & J. Barnes (San Francisco, CA:
Bañados, E., Connor, T., Stern, D., et al. 2018, ApJL, 856, L25
Bisogni, S., Lusso, E., Civano, F., et al. 2021, A&A, 655, A109
Brandt, W. N., Laor, A., & Wills, B. J. 2000, ApJ, 528, 637
Broos, P. S., Feigelson, E. D., Townsley, L. K., et al. 2007, ApJS, 169, 353
Cash, W. 1979, ApJ, 228, 939
Connor, T., Bañados, E., Mazzucchelli, C., et al. 2020, ApJ, 900, 189
Connor, T., Bañados, E., Stern, D., et al. 2019, ApJ, 887, 171
Fan, X., Wang, F., Yang, J., et al. 2019, ApJL, 870, L11
Gabriel, C., Denby, M., Fyfe, D. J., et al. 2004, in ASP Conf. Ser. 314,
   Astronomical Data Analysis Software and Systems XIII, ed. F. Ochsenbein,
   M. G. Allen, & D. Egret (San Francisco, CA: ASP), 759
Gallagher, S. C., Brandt, W. N., Chartas, G., et al. 2002, ApJ, 567, 37
Gallerani, S., Zappacosta, L., Orofino, M. C., et al. 2017, MNRAS, 467, 3590
Gibson, R. R., Brandt, W. N., Gallagher, S. C., et al. 2009, ApJ, 696, 924
Gibson, R. R., Brandt, W. N., & Schneider, D. P. 2008, ApJ, 685, 773
Green, P. J., Aldcroft, T. L., Mathur, S., et al. 2001, ApJ, 558, 109
Just, D. W., Brandt, W. N., Shemmer, O., et al. 2007, ApJ, 665, 1004
Kalberla, P. M. W., Burton, W. B., Hartmann, D., et al. 2005, A&A, 440, 775
Kollatschny, W., Schartel, N., Zetzl, M., et al. 2016, A&A, 585, A18
Laurenti, M., Piconcelli, E., Zappacosta, L., et al. 2021, arXiv:2110.06939
Leighly, K. M., Halpern, J. P., Jenkins, E. B., et al. 2007, ApJ, 663, 103
Liu, H., Luo, B., Brandt, W. N., et al. 2018, ApJ, 859, 113
Luo, B., Brandt, W. N., Alexander, D. M., et al. 2013, ApJ, 772, 153
Luo, B., Brandt, W. N., Alexander, D. M., et al. 2014, ApJ, 794, 70
```

```
Lusso, E., & Risaliti, G. 2017, A&A, 602, A79
Martocchia, S., Piconcelli, E., Zappacosta, L., et al. 2017, A&A, 608, A51
Matsuoka, Y., Iwasawa, K., Onoue, M., et al. 2019, ApJ, 883, 183
Ménard, B., & Chelouche, D. 2009, MNRAS, 393, 808
Moretti, A., Ballo, L., Braito, V., et al. 2014, A&A, 563, A46
Nanni, R., Gilli, R., Vignali, C., et al. 2018, A&A, 614, A121
Nanni, R., Vignali, C., Gilli, R., et al. 2017, A&A, 603, A128
Nardini, E., Lusso, E., Risaliti, G., et al. 2019, A&A, 632, A109
Page, K. L., Reeves, J. N., O'Brien, P. T., et al. 2005, MNRAS, 364, 195
Page, M. J., Simpson, C., Mortlock, D. J., et al. 2014, MNRAS, 440, L91
Pons, E., McMahon, R. G., Banerji, M., et al. 2020, MNRAS, 491, 3884
Proga, D. 2005, ApJL, 630, L9
Reed, S. L., Banerji, M., Becker, G. D., et al. 2019, arXiv:1901.07456
Schindler, J.-T., Farina, E. P., Bañados, E., et al. 2020, ApJ, 905, 51
Sameer, Brandt, W. N., Anderson, S., et al. 2019, MNRAS, 482, 1121
Scott, A. E., Stewart, G. C., Mateos, S., et al. 2011, MNRAS, 417, 992
Shemmer, O., Brandt, W. N., Schneider, D. P., et al. 2006, ApJ, 644, 86
Shen, Y., Wu, J., Jiang, L., et al. 2019, ApJ, 873, 35
Timlin, J. D., Brandt, W. N., Ni, Q., et al. 2020, MNRAS, 492, 719
Venemans, B. P., Bañados, E., Decarli, R., et al. 2015, ApJ, 801, L11
Vignali, C., Brandt, W. N., Schneider, D. P., et al. 2005, AJ, 129, 2519
Vito, F., Brandt, W. N., Bauer, F. E., et al. 2019, A&A, 630, A118
Vito, F., Brandt, W. N., Ricci, F., et al. 2021, A&A, 649, A133
Wang, F., Fan, X., Yang, J., et al. 2021, ApJ, 908, 53
Wang, F., Yang, J., Fan, X., et al. 2019, ApJ, 884, 30
Weisskopf, M. C., Wu, K., Trimble, V., et al. 2007, ApJ, 657, 1026
Yang, J., Venemans, B., Wang, F., et al. 2019a, ApJ, 880, 153
Yang, J., Wang, F., Fan, X., et al. 2019b, AJ, 157, 236
Yang, J., Wang, F., Fan, X., et al. 2021, ApJ, 923, 262
Yue, M., Yang, J., Fan, X., et al. 2021, ApJ, 917, 99
```